1. Supplementary Figures

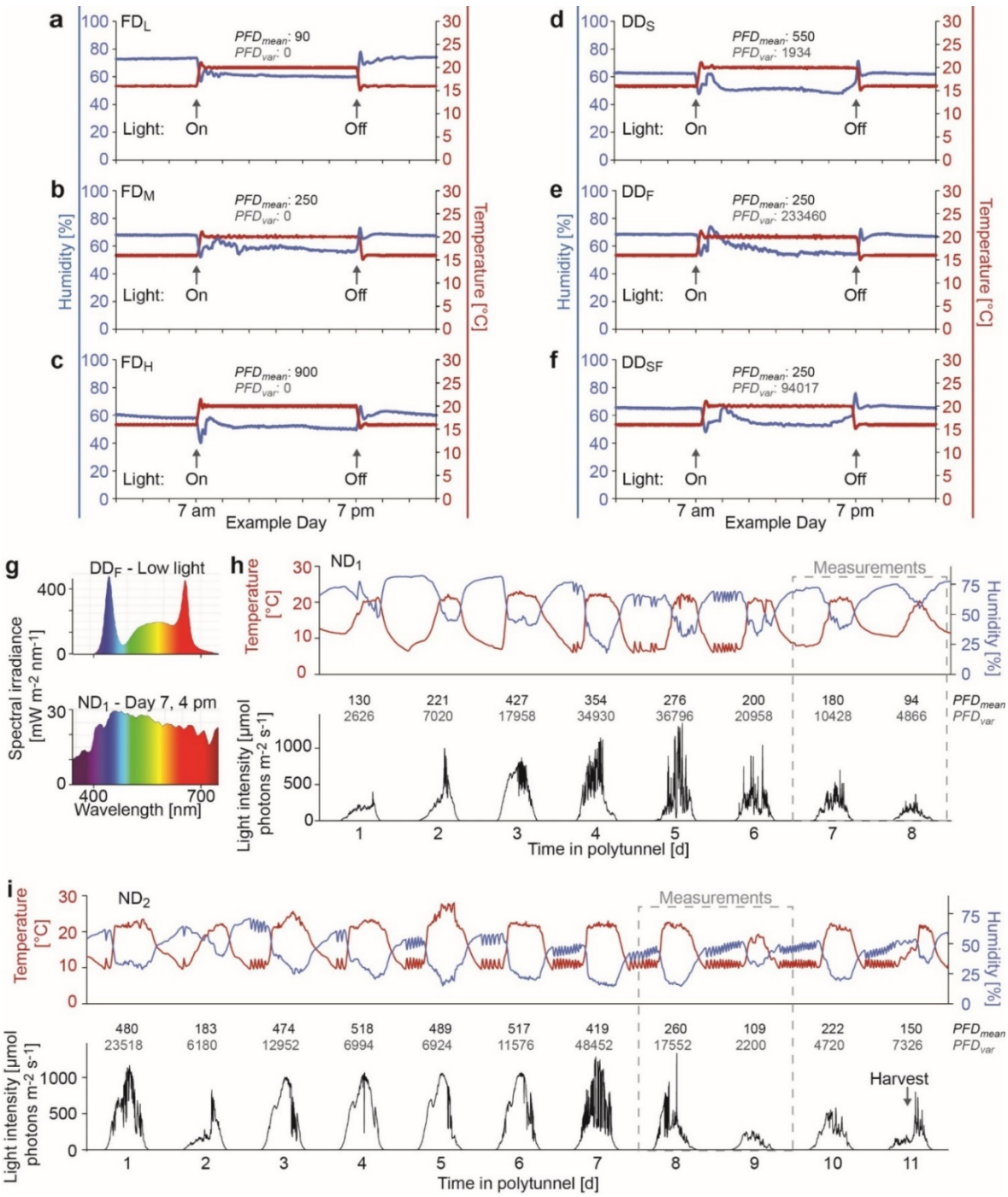

Supplemental Fig. 1 Light and climate traces of the different growth environments.
a-f, Representative daily traces of humidity (left axis, blue) and temperature (right axis, red) recorded in the phytotron (flat day low: FD_L, a; medium: FD_M, b; high: FD_H, c; dynamic day sinusoidal: DD_S, d; fluctuating: DD_F, e; sinusoidal fluctuating: DD_{SF}, f). **g,** Representative spectral composition of light in the phytotron (here: DD_F during low light phase) and in the polytunnel (here: ND_1 on day 7 at 4 pm). **h-i,** Temperature (left axis, red), humidity (right axis, blue, upper panels) and light intensity (lower panels, black) of ND_1 (h, 21.03.-28.03.2019) and ND_2 (i, 04.04.-14.04.2019) in the polytunnel. Average and variable daily light intensities (PFD_{mean} in black and PFD_{var} in grey, respectively) are displayed. PFD_{var} is calculated as the sum of all light intensity changes over the day. An overview of the light parameters is provided in Supplemental table Fig1a-b_SFig1.

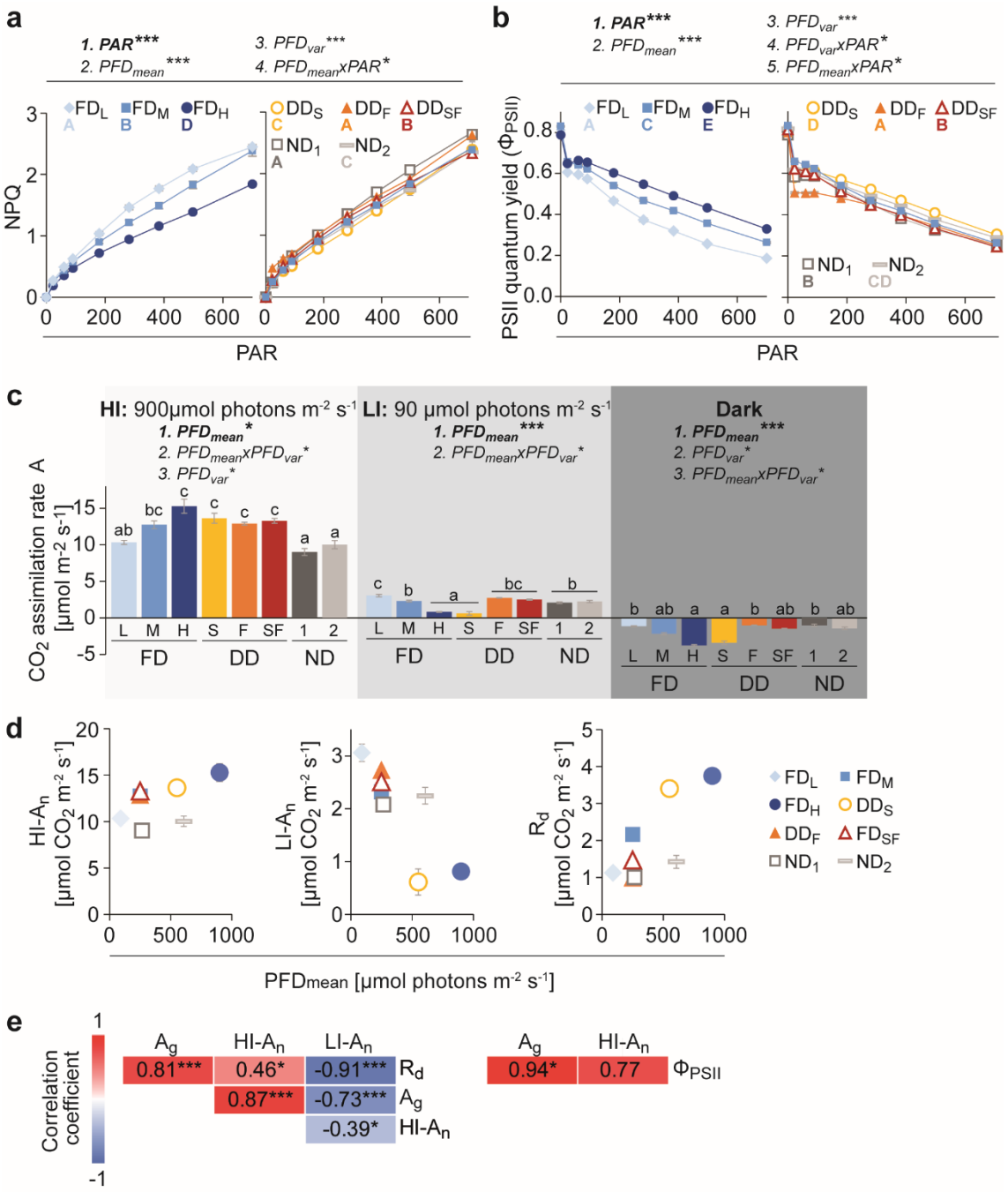

Supplemental Fig. 2 Steady state photosynthesis is strongly shaped by growth light intensity and to a lesser extent by light variability.

a-b, Non-photochemical quenching (NPQ, a) and PSII quantum efficiency (Φ_{PSII}; b) as a function of photosynthetically active radiation (PAR) depending on 8 different growth environments (FD_L, FD_M, FD_H, DD_S, DD_F, DD_{SF}, ND_1, ND_2; Fig. 1a-b) **c**, Whole rosette CO_2 assimilation rates (A_n) after 10 min of 900 µmol photons m^{-2} s^{-1} (High irradiation: HI), 10 min of 90 µmol photons m^{-2} s^{-1} (Low irradiation: LI) and after 5 min darkness. **a-c**, Averages of n = 5-7 ± SE are shown. An ANCOVA was used to distinguish effects of PAR (a-b), PFD_{mean} (a-c), PFD_{var} (a-c) and their interactions. Factors are ranked according to their strength. Asterisks indicate statistical significance with * p< 0.05 and *** p<0.0001. Capital letters below the legends (a-b) or lowercase letters above the graphs (c) indicate different statistical groups. Detailed statistical analysis can be found in Supplemental Table SFig2a-b or Table Fig1d_SFig2c, respectively. **d**, CO_2 assimilation rates ($HI\text{-}A_n$ and $LI\text{-}A_n$) and respiration (CO_2 release in the dark, R_d) as shown in (c) as a function of PFD_{mean}. **e,** Spearman's correlation matrix between net CO_2 exchange parameters and gross assimilation rates in HI (A_g, calculated as $HI\text{-}A_n+R_d$; left panel) and between Φ_{PSII} at 700 µmol photons m^{-2} s^{-1} and A_g and $HI\text{-}A_n$ (right panel). Asterisks indicate statistical significance with * p< 0.05 and *** p<0.0001.

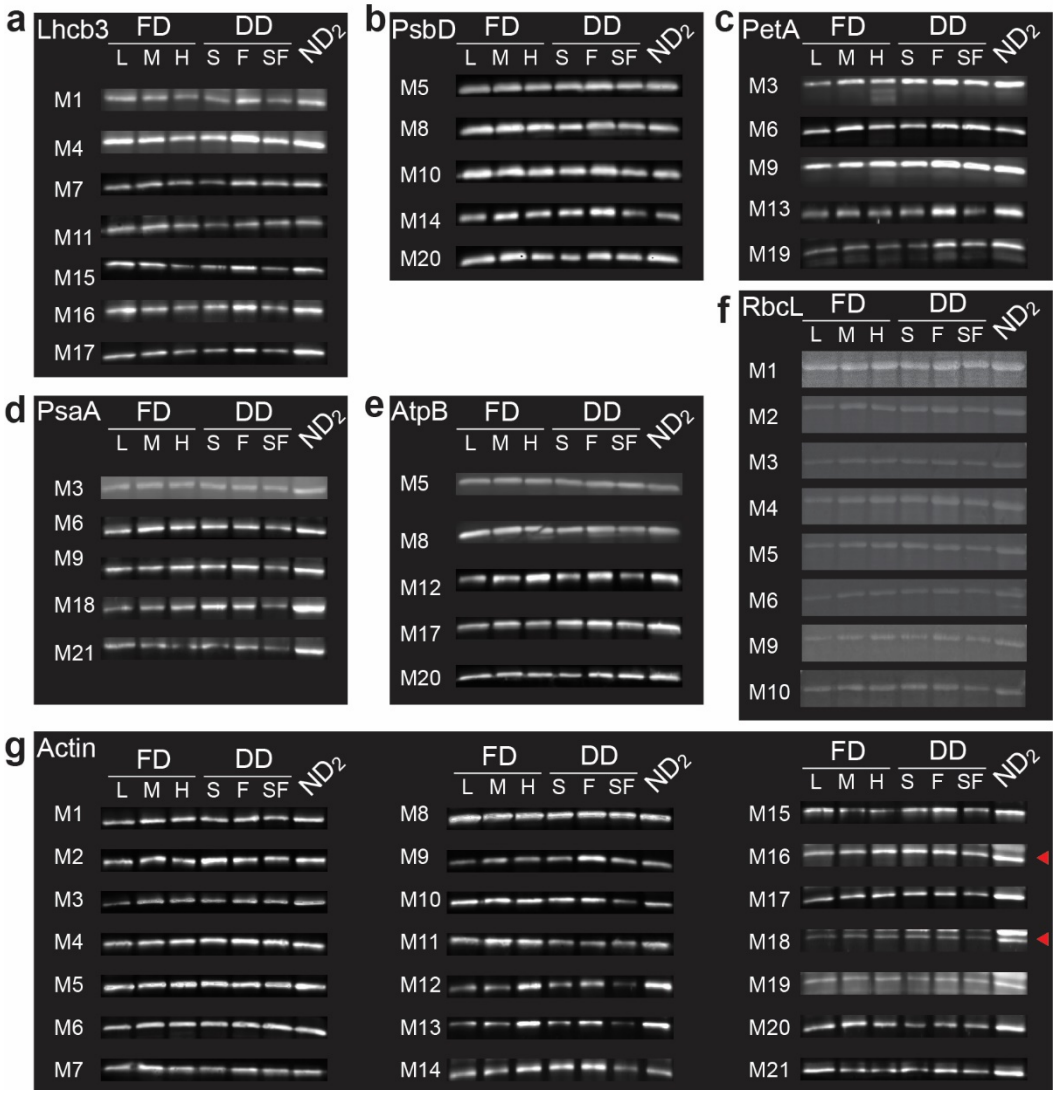

Supplemental Fig. 3 Immunoblots of selected subunits of photosynthetic complexes.
Immunoblots of total WT leaf proteins from 7 different growth environments (FD_L, FD_M, FD_H, DD_S, DD_F, DD_{SF}, ND_2; Fig. 1a-b) using specific antibodies against Lhcb3 (a), PsbD (b), PetA (c), PsaA (d), AtpB (e), Actin (g) and Ponceau stained membranes for Rubisco (f). The same membranes (M) as in a-f were used for incubation with anti-actin. The signal was quantified via ImageJ and values can be found in Supplemental Table SFig3_SFig4b.

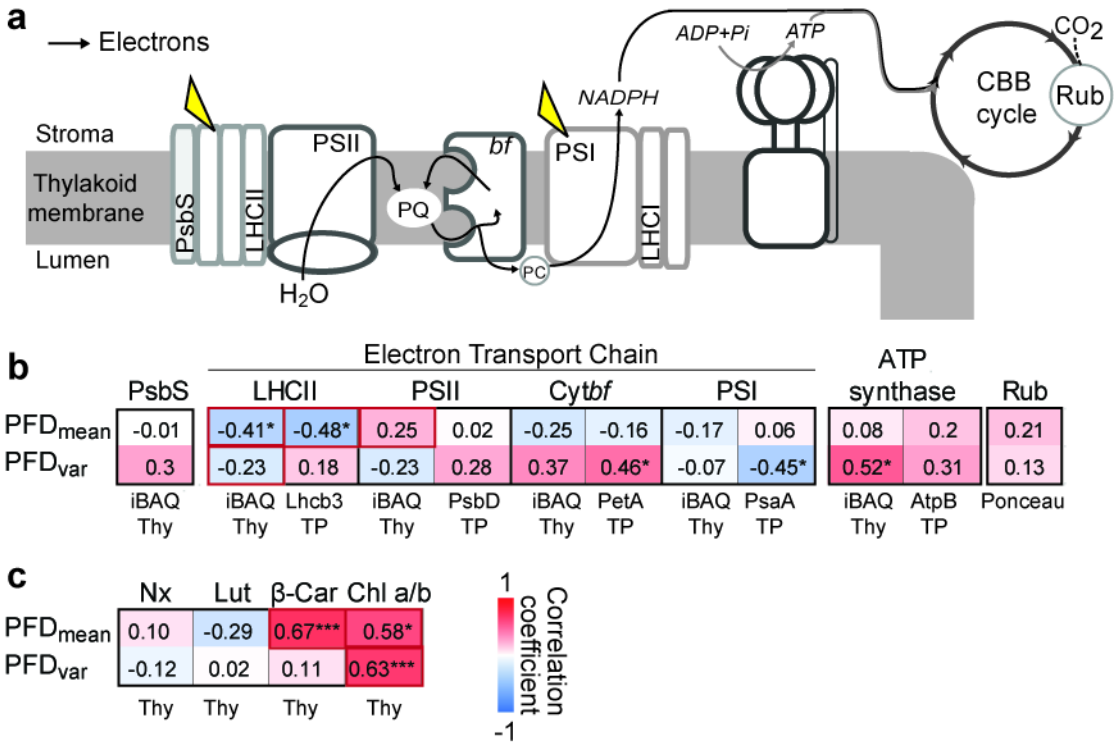

Supplemental Fig. 4 Effects of growth light intensity and variability on photosynthetic complexes and pigments.

a, Scheme of photosynthetic complexes: PsbS – photosystem II subunit S, LHCII – light harvesting complex II, PSII – photosystem II, PQ – plastoquinol, *bf* – cytochrome b_6f, PC – plastocyanin, PSI – photosystem I and LHCI – light harvesting complex I and Calvin Benson Bassham (CBB) cycle with Rub – Rubisco. **b-c,** Spearman's correlation analysis of photosynthetic complexes (b) or pigments (c) of WT from 7 different growth environments (FD_L, FD_M, FD_H, DD_S, DD_F, DD_{SF}, ND_2; Fig. 1a-b) with average and variable photon flux densities (PFD_{mean} and PFD_{var}, respectively). Averages of n = 4 (Thy) or n = 5-8 (TP) were used and asterisks indicate significant correlations with * $p<0.05$ and *** $p<0.0001$. Red boxes indicate significant differences found by multiple regression analysis using PFD_{mean} and PFD_{var} as covariates ($p<0.05$, detailed analysis in Supplemental Table SFig4b_2, Supplemental Table SFig4b_3 and Supplemental Table SFig4c). Protein levels were determined either from isolated thylakoids (Thy) by mass spectrometry (iBAQ: intensity-based absolute quantification, all data in Supplemental Table_SFig4b_1) or total leaf protein (TP) by immunoblots normalized on Actin (blots shown in Supplemental Fig. 3, all data in Supplemental Table SFig3_SFig4b). Pigment content was determined from isolated thylakoids by HPLC and average data can be found in Supplemental Table Fig1e-f_SFig4c.

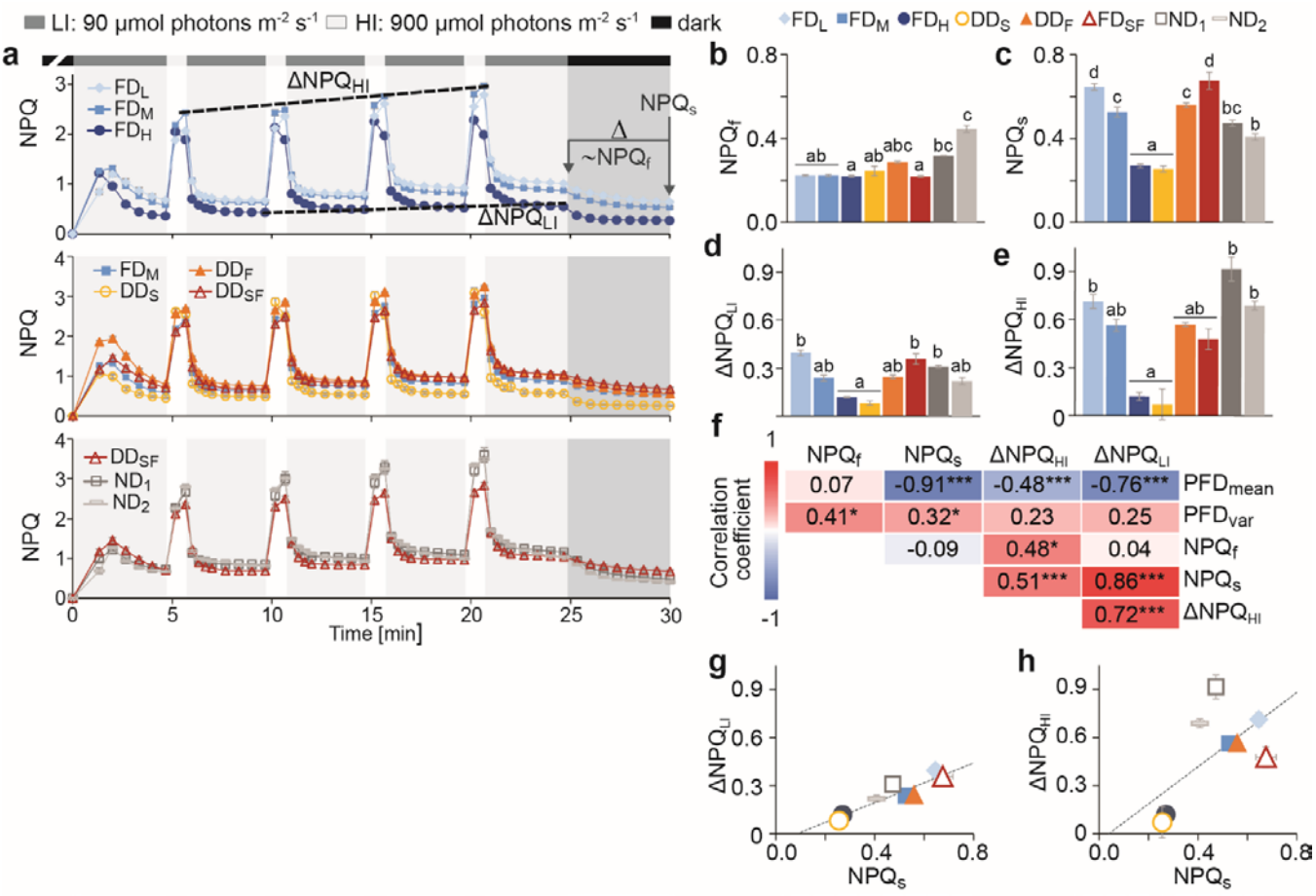

Supplemental Fig. 5 Growth light intensity, variability as well as additional environmental factors shape dynamic NPQ.

a, NPQ traces of 30 min dark-acclimated WT plants from the different growth environments (FD_L, FD_M, FD_H, DD_S, DD_F, DD_{SF}, ND_1, ND_2; Fig. 1a-b) exposed to four iterations of 4 min 90 (low irradiance, LI) and 1 min 900 µmol photons m^{-2} s^{-1} (high irradiance, HI), followed by a 5 min dark phase. Averages of n = 5-7 ± SE are shown. Statistical analyses can be found in Supplemental Table_SFig5a. **b-c,** Bar graphs displaying NPQ composition after the final light fluctuation: fast NPQ (NPQ_f; b) relaxes and slow NPQ (NPQ_s; c) remains after 5 min darkness. **d-e,** Bar graphs representing ΔNPQ_{LI} (d) and ΔNPQ_{HI} (e) defined as the increase in NPQ between the first and the last LI and HI phase as in a. **b-e,** Different lowercase letters above the graph indicate significant differences between conditions as determined by one-way ANOVA and subsequent Tukey multiple comparison test in case of normal distribution (c) or Student-Newman-Keuls test (b, d-e). **f,** Spearman's correlation matrix for NPQ_f, NPQ_s, ΔNPQ_{LI} and ΔNPQ_{HI} between each other and PFD_{mean} and PFD_{var}. Asterisks indicate significant correlations with * $p<0.05$ and *** $p<0.0001$. **g-h**, ΔNPQ_{LI} (g) and ΔNPQ_{HI} (h) plotted as a function of NPQ_s. Dotted lines represent the linear fit. **a-h,** Averages of n = 5-7 ± SE are shown.

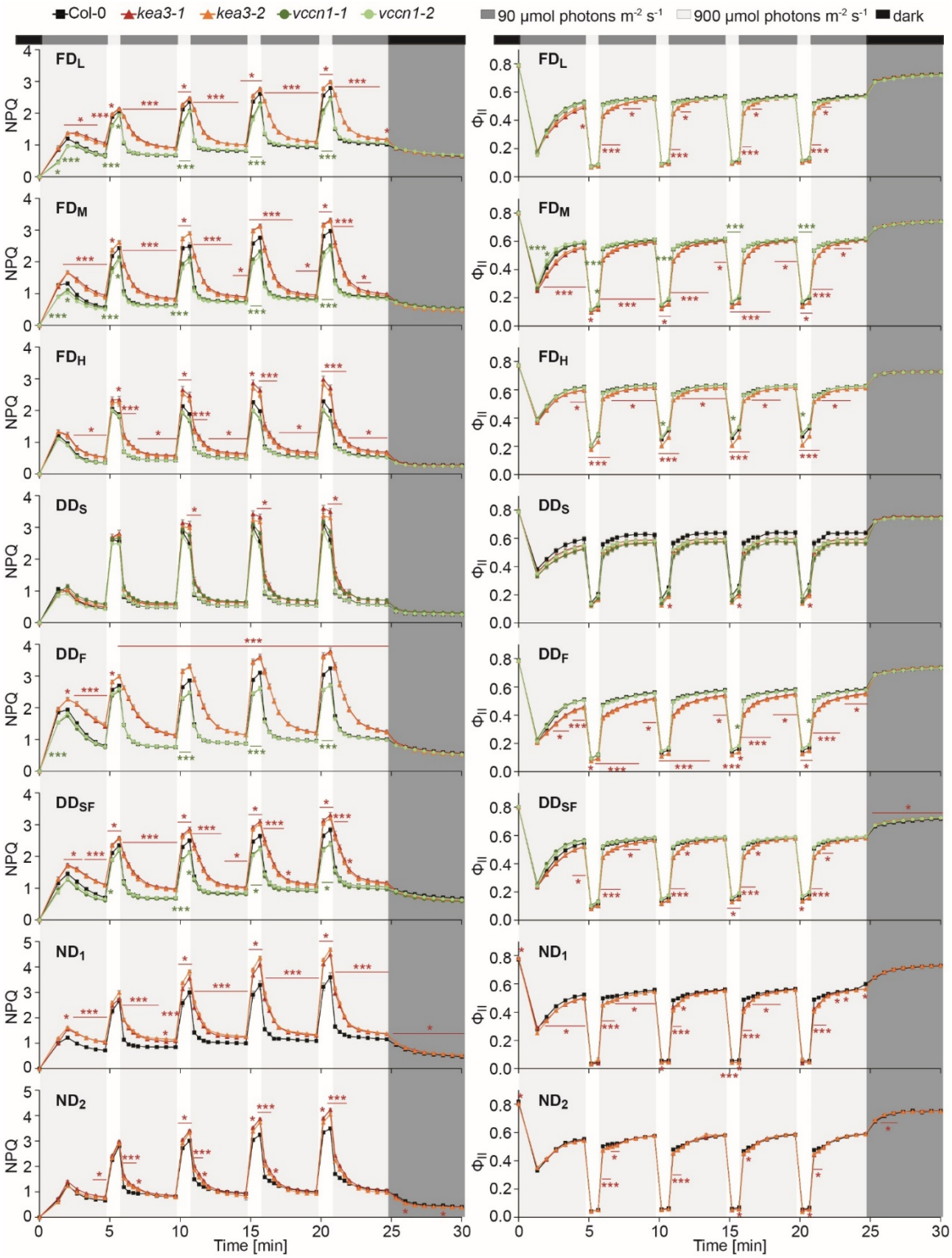

Supplemental Fig. 6 Effects of different growth environments on NPQ and Φ_{II} of WT, *kea3* and *vccn1* during light fluctuations.

Mature rosettes of WT and two mutant alleles each of *kea3* and *vccn1* were analyzed from 8 different growth environments (FD_L, FD_M, FD_H, DD_S, DD_F, DD_{SF}, ND_1, ND_2; Fig. 1a-b) by Chl *a* fluorescence analysis (as in Supplemental Fig. 5a). NPQ and Φ_{PSII} traces (left and right panel, respectively) are shown of 30 min dark-acclimated plants exposed to iterations of 4 min 90 and 1 min 900 µmol photons m^{-2} s^{-1}, followed by a 5 min dark phase. Averages of n = 5-7 ± SE are shown. Asterisks in the corresponding color indicate significant differences of both mutant alleles of *kea3* or *vccn1* as compared to WT (red: *kea3*, green: *vccn1*), determined by one-way ANOVA and subsequent Tukey multiple comparison test with * p<0.5 and *** p<0.0001.

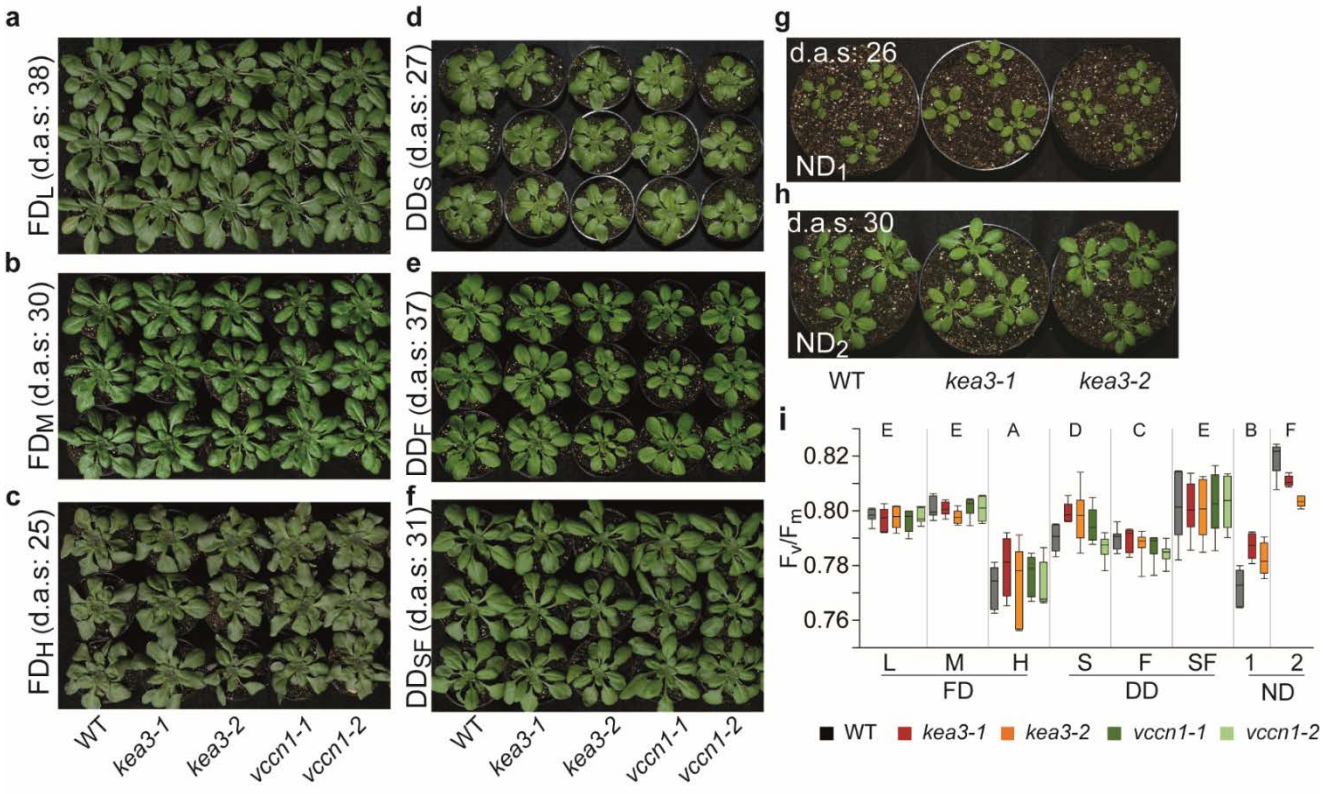

Supplemental Fig. 7 Effects of different growth environments on visual phenotypes and Fv/Fm of WT, *kea3* and *vccn1*.

a-h, Pictures of WT and two mutant alleles each of *kea3* and *vccn1* from the 8 different growth environments (FD_L, FD_M, FD_H, DD_S, DD_F, DD_{SF}, ND_1, ND_2; Fig. 1a-b) at indicated days after sowing (d.a.s.). **i,** Maximum quantum efficiency of PSII (Fv/Fm). Averages of n = 5-7 ± SE per genotype and condition are shown. Capital letters above the boxes indicate significant differences between conditions as determined by two-way ANOVA and Student-Newman-Keuls test.

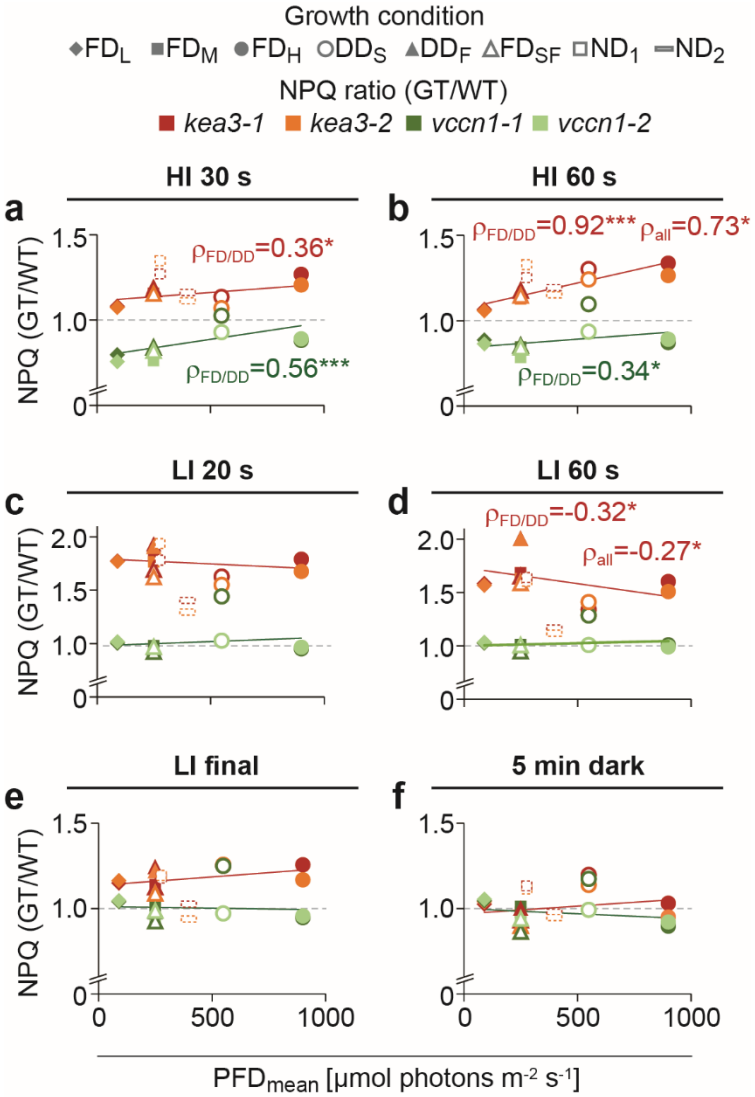

Supplemental Figure 8 Growth light intensity affects the dynamic NPQ phenotypes of *kea3* and *vccn1* particularly during high light phases.

a-f, NPQ ratio of *kea3*/WT or *vccn1*/WT from 8 different growth conditions (FD_L, FD_M, FD_H, DD_S, DD_F, DD_{SF}, ND_1, ND_2; Fig. 1a-b) at 6 different time points during the fluctuating light regime shown in Fig. 2: After 30 s (a) and 60 s (b) at high irradiance (HI; 900 µmol photons m^{-2} s^{-1}) and 20s (c) or 60s (d) at the subsequent low irradiance phase (LI; 90 µmol photons m^{-2} s^{-1}) during the 3rd light fluctuations, as well as at the end of the final LI phase (e) and after 5 min darkness (f) as a function of PFD_{mean}. Lines in the corresponding color represent the linear fit through all *kea3* (red) or *vccn1* (green) NPQ ratio data points and Pearson correlation coefficients are given for all statistically significant correlations between the NPQ ratio and PFD_{mean} with * $p<0.05$ and *** $p<0.0001$ (*kea3*: red; *vccn1*: green), either for all growth conditions (ρ_{all}) or only for phytotron-grown plants ($\rho_{FD/DD}$).

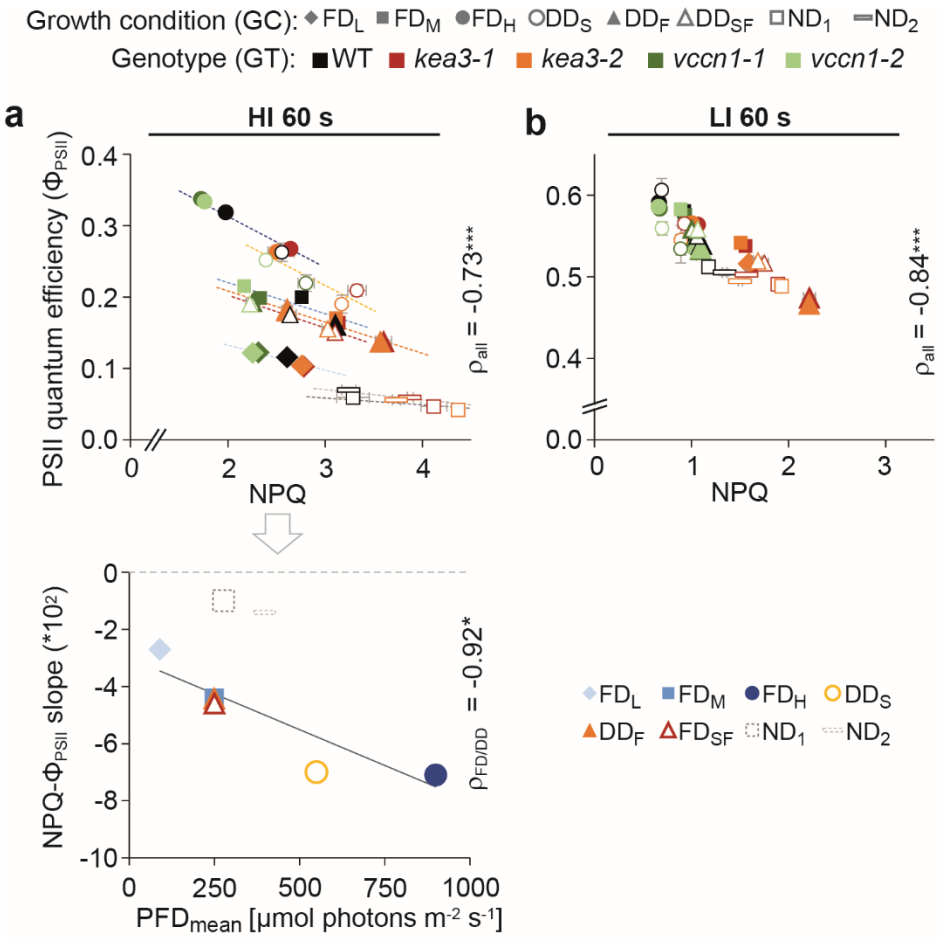

Supplemental Fig. 9 Growth light intensity determines the Φ_{PSII}-NPQ relationship.
a-b, Φ_{PSII} plotted against NPQ of WT, *kea3* and *vccn1* lines from 8 different growth conditions (FD_L, FD_M, FD_H, DD_S, DD_F, DD_{SF}, ND_1, ND_2; Fig. 1a-b) at 60 s after transfer from LI to HI (HI 60 s; a, upper panel) and 60 s after transfer form HI to LI (LI 60 s, b) during the third light fluctuation as shown in Fig. 2a. Colored dashed lines indicate environment specific slopes according to the figure's color scale of conditions (a, upper panel), showing a strong correlation with PFD_{mean} (a, lower panel). Averages of n = 3-7 ± SE are shown. Pearson correlation coefficient ρ is given for all points (ρ_{all}) or phytotron grown plants only ($\rho_{FD/DD}$) and asterisks indicate significant correlation with * $p<0.05$ and *** $p<0.0001$. Environmental specific slopes for all time points and for different groups of points with corresponding ρ can be found in Supplemental Table Fig3_SFig9.

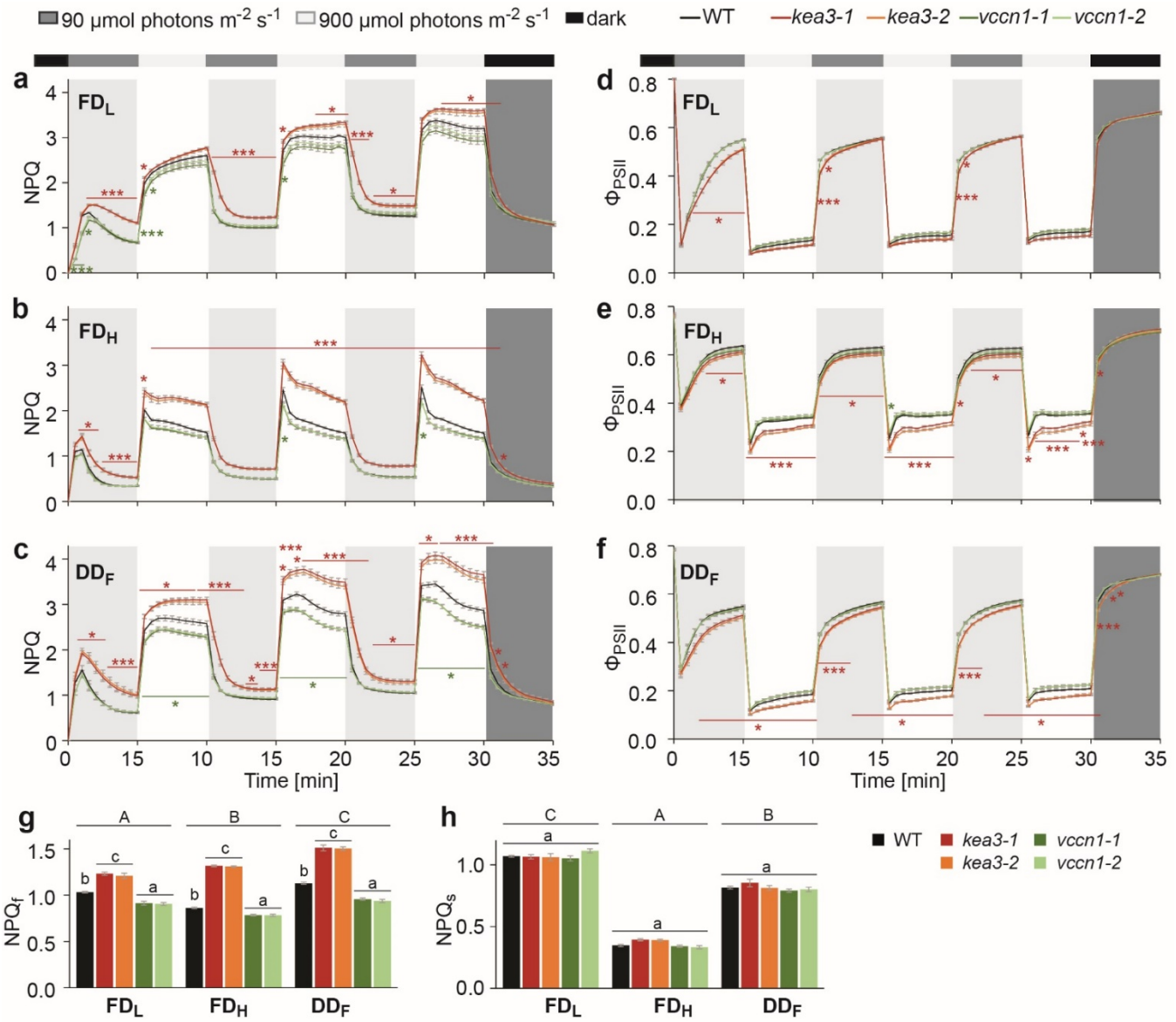

Supplemental Fig. 10 Photosynthetic response of WT, *kea3* and *vccn1* during fluctuations with longer (5 min) HI periods.

a-f, NPQ (a-c) and Φ_{PSII} (d-f) traces of WT and two mutant alleles each of *kea3* and *vccn1* exposed to three iterations of 5 min LI and 5 min HI, followed by a 5 min dark phase. Asterisks in the corresponding color indicate significant differences of both mutant alleles of *kea3* and *vccn1* as compared to WT, determined by one-way ANOVA and subsequent Tukey multiple comparison test with * $p<0.5$ and *** $p<0.0001$ (red: *kea3*; green: *vccn1*). **g-h,** Bar graphs displaying NPQ composition after the final light fluctuation: fast NPQ (NPQ_f; g) relaxes within 5 min darkness, slow NPQ (NPQ_s; h) has slower relaxation kinetics. Averages of n = 5-6 ± SE are shown. Capital letters indicate significant differences between environments and lowercase letters significant differences between the genotypes within a given environment as determined via two-way ANOVA and subsequent Tukey (g) or Student-Newman-Keuls tests (h) with $p<0.05$.

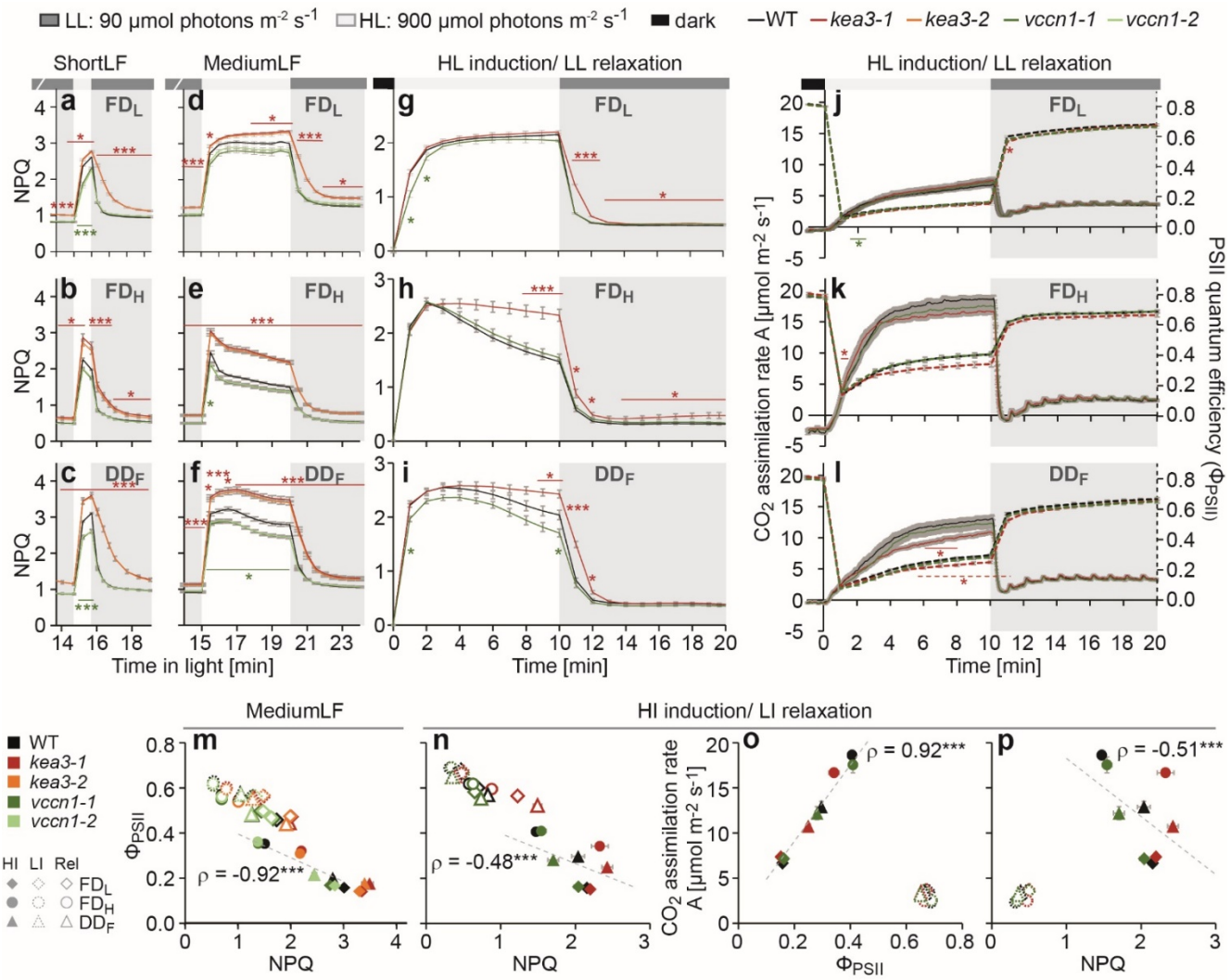

Supplemental Fig. 11 Photosynthetic response of WT, *kea3* and *vccn1* to different lengths of fluctuations.

a-i, NPQ response during a 5 min HI-LI fluctuation as shown in Fig. 2 (short light fluctuations, ShortLF; a-c), 10 min as shown in Supplemental Fig. 10 (medium light fluctuations, MediumLF; d-f) or 20 min induction in HI with subsequent LI relaxation (g-i) for plants grown in FD_L (a, d, g), FD_H (b, e, h) and DD_F (c, f, i). **j-k,** Single leaf CO_2 assimilation rate (left axes) and PSII quantum efficiency (Φ_{PSII}, right axes) during HI induction/LI relaxation for plants grown in FD_L (j), FD_H (k) and DD_F (l). **a-l,** Asterisks in the corresponding color indicate significant difference of both mutant alleles of *kea3* and *vccn1* as compared to WT, determined by one-way ANOVA and subsequent Tukey multiple comparison test with * $p<0.5$ and *** $p<0.0001$. **m-n,** Φ_{PSII} plotted against NPQ at the end of HI and LI periods and after 60 s during relaxation in LI (Rel) as in d-f (m) or g-i (n). **o-p,** CO_2 assimilation rate plotted against Φ_{PSII} as in j-l (o) or NPQ as in g-l (p). **m-p,** Dotted lines represent the linear fit using only the HI values. Pearson correlation factor ρ for HI is shown with asterisks indicating statistical significance (*** $p<0.0001$). All slopes of the linear fit and the Pearson correlation coefficients are given for different groups of points in Supplemental Table_SFig11. **a-p,** Averages of n = 5-9 ± SE are shown.

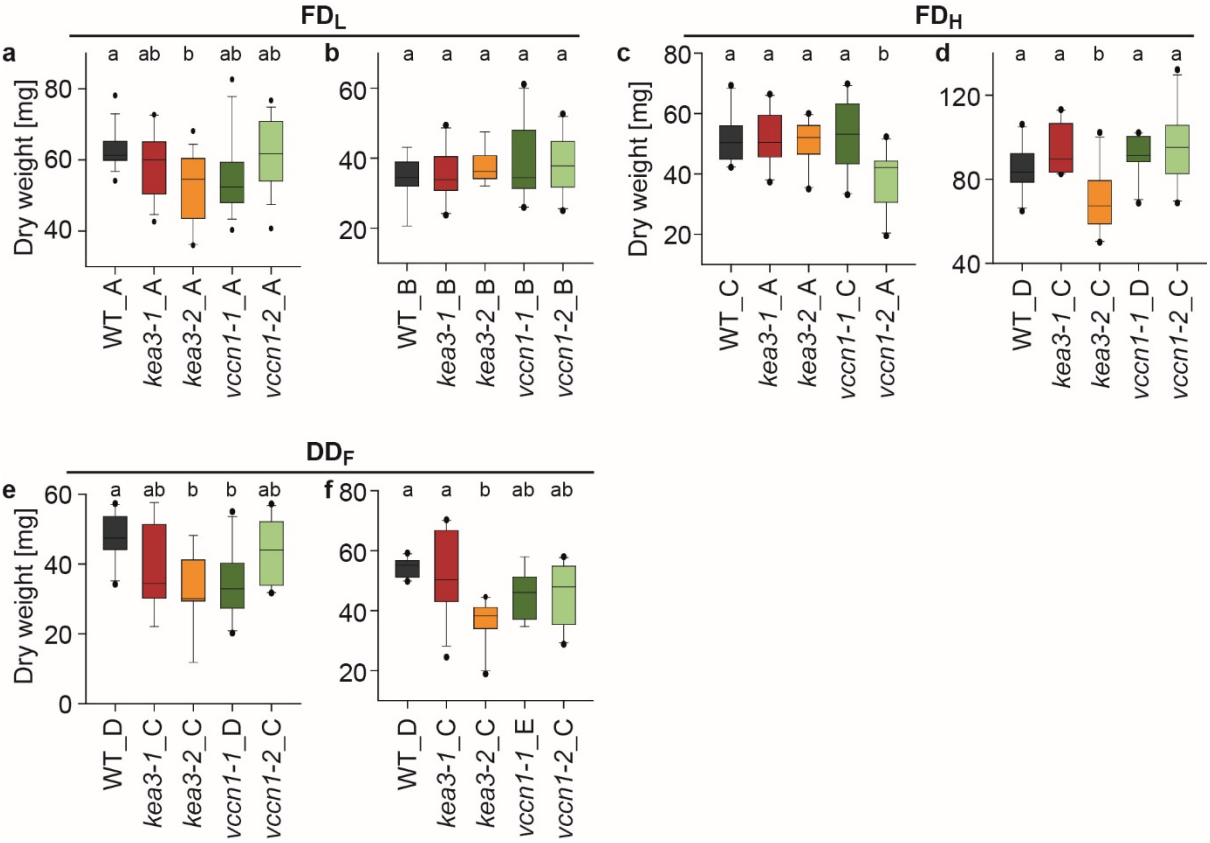

Supplemental Fig. 12 Dry weight of WT, *kea3* and *vccn1* from three different light conditions.
a-f, Dry weight of WT and thylakoid ion transport mutants 50 and 35 days after sowing (d.a.s.) in FD_L (a, b), 25 and 24 d.a.s. in FD_H (c, d) and 33 and 39 d.a.s. in DD_F (e, f). Box plots represent n = 8-14. Different seed stocks are indicated by capital letters after the genotype. Lowercase letters indicate significant differences between genotypes as determined by one-way ANOVA and subsequent Tukey multiple comparison or Student-Newman-Keuls tests ($p<0.05$).

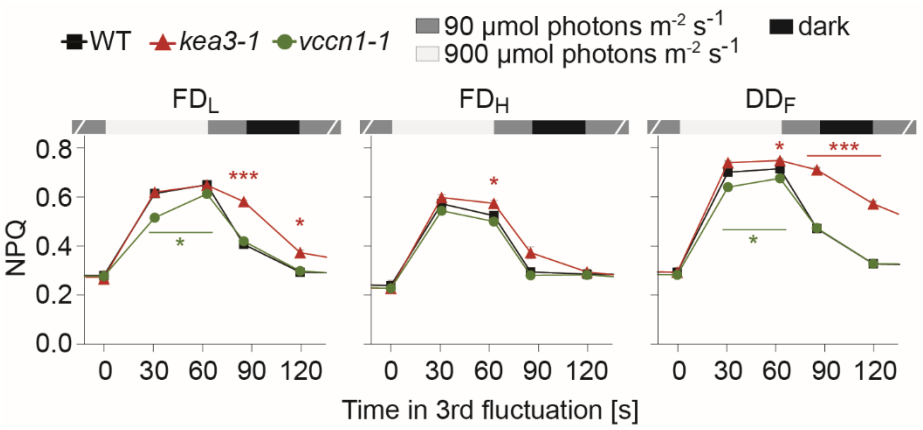

Supplemental Fig. 13 NPQ under short light fluctuations with 30 s dark interval

NPQ traces of WT, *kea3-1* and *vccn1-1* grown in FD_L (left panel), FD_H (middle panel) or DD_F (right panel) during the third light fluctuation as in Fig. 2a with the exception that a 20 s dark phase was introduced 20 s after shift from HI to LI. Averages of n = 3 ± SE are shown. Asterisks in the corresponding color indicate significant difference of *kea3-1* and *vccn1-1* to WT, determined by one-way ANOVA and subsequent Tukey multiple comparison test with * $p<0.5$ and *** $p<0.0001$.

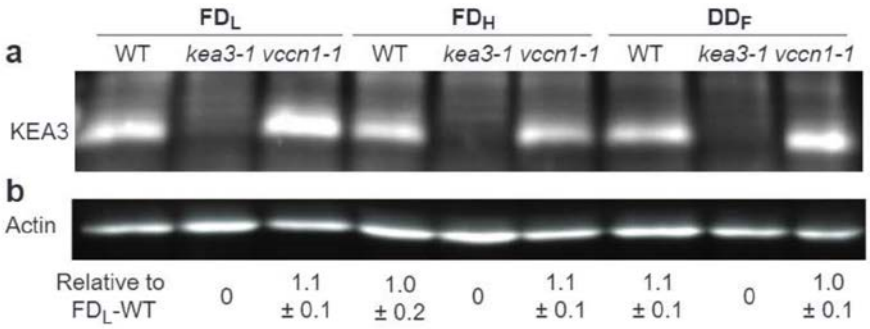

Supplemental Fig. 14 Light acclimation does not affect levels of KEA3.

a-b, Representative results of immunoblots from total leaf protein of WT, *kea3-1* and *vccn1-1* from the three different environments FD_L, FD_H and DD_F, hybridized with specific antibodies against KEA3 (a) and Actin (b). Signals of KEA3 were normalized to Actin and averages relative to FD_L grown WT with n = 5 ± SE are displayed below. The signal was quantified via ImageJ and all values can be found in Supplemental Table_SFig14.

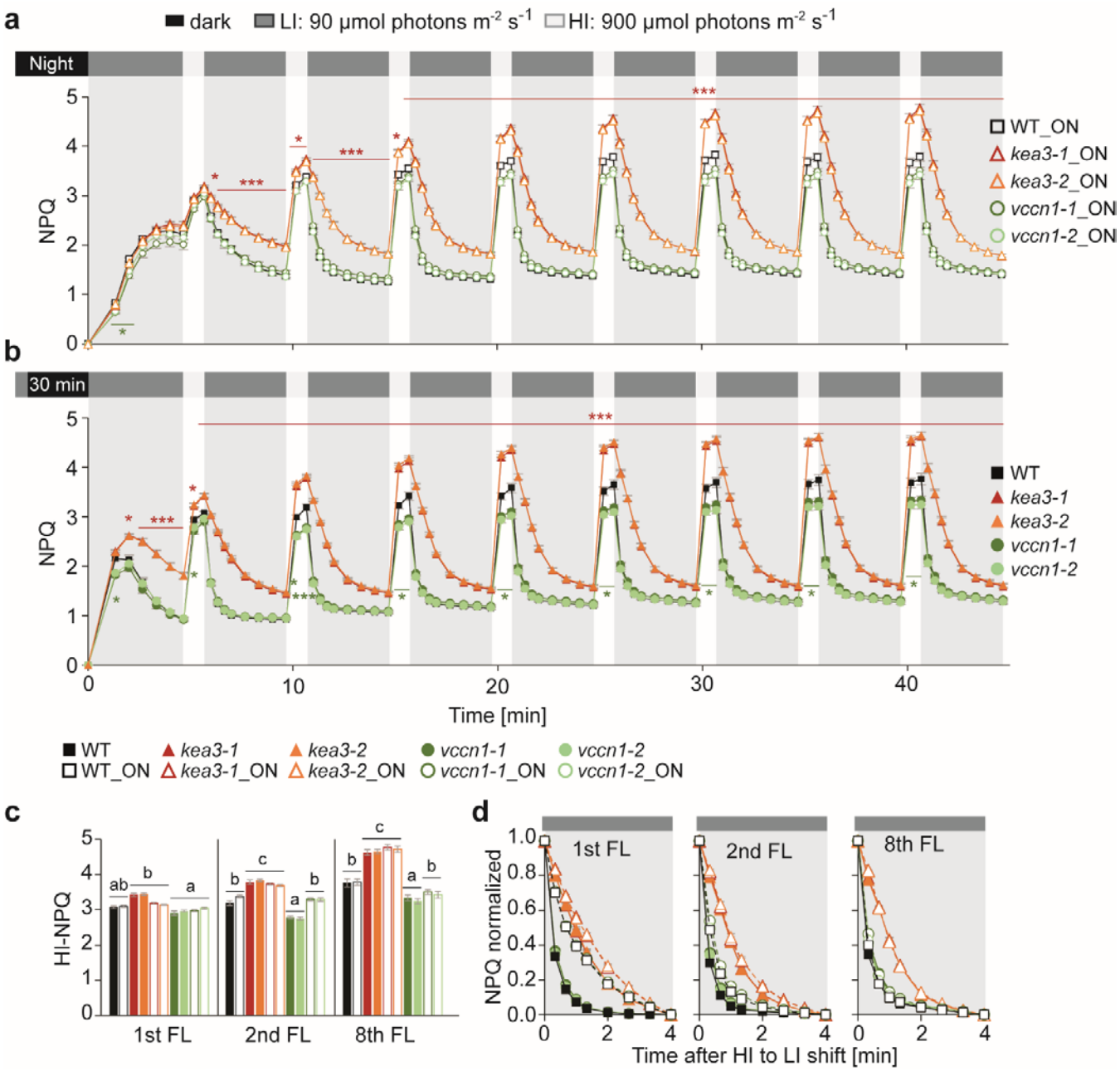

Supplemental Fig. 15 Effects of different dark treatments on NPQ dynamics during light fluctuations.

a-b, NPQ was determined of DD_F grown WT and two mutant alleles each of *kea3* and *vccn1* during 8 iterations of 4 min LI (low irradiance: 90 µmol photons m^{-2} s^{-1}) and 1 min HI (high irradiance: 900 µmol photons m^{-2} s^{-1}). Plants were either measured directly at the end of their nightly dark phase (ON, a) or at least two 2 h into the photoperiod with a 30 min dark acclimation phase preceding the NPQ measurements (b). Averages of n = 6 ± SE are shown. Asterisks in the corresponding color indicate significant differences of both mutant alleles of *kea3* and *vccn1* as compared to WT, determined by one-way ANOVA and subsequent Tukey multiple comparison test with * p<0.5 and *** p<0.0001. **c-d,** NPQ after 1 min HI (c) or its relaxation kinetics in LI (d) of ON and 30 min dark treated plants for the first 2 fluctuations after the dark treatment and at the end (i.e., 8th fluctuation). For understanding the relaxation kinetics in LI, NPQ was normalized to the amplitude of the decay. Average is shown for n = 6 ± SE. Different lowercase letters above the graph indicate significant differences between genotypes and/ or conditions as determined by one-way ANOVA and subsequent Tukey multiple comparison test.

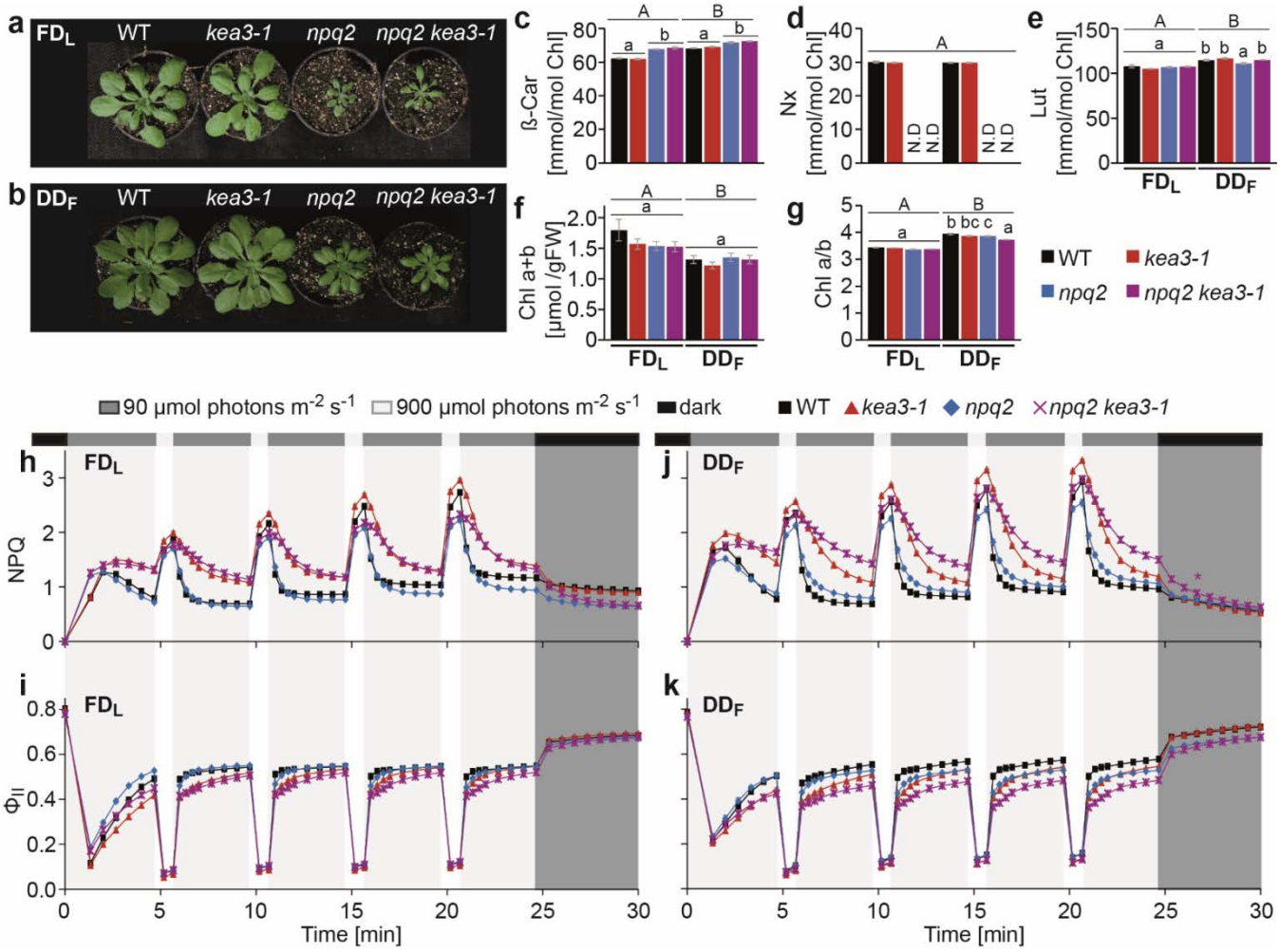

Supplemental Fig. 16 Analysis of dynamic photosynthesis in *npq2* and *npq2 kea3-1* mutants.
a-b, Pictures of WT, *kea3-1*, *npq2* and *npq2 kea3-1* mutants grown in FD_L (a) and DD_F (b) at the age of analysis (FD_L: 31 d.a.s., DD_F: 39 d.a.s). **c-g,** Pigment composition of plants after 6 h growth light depicted as mmol per mol Chl except for f, which depicts total chlorophyll as µmol per gram fresh weight and g, which presents the Chl *a*/*b* ratio. Averages of n = 5 ± SE are shown. Different capital letters above the graph indicate significant differences between growth condition, and lowercase letters significant differences between genotypes within one condition as determined by two-way ANOVA and subsequent Tukey multiple comparison or Student-Newman-Keuls tests. **h-k,** NPQ (h, j) and Φ_{PSII} (i, k) traces of plants from FD_L (h, i) or DD_F (j, k) during 4 iterations of 4 min LI (low irradiance: 90 µmol photons m^{-2} s^{-1}) and 1 min HI (high irradiance: 900 µmol photons m^{-2} s^{-1}). Averages of n = 6 ± SE are shown. Statistical analysis can be found in Supplemental Table_SFig16h-k.

2. Supplementary Results and Discussion

Environmental effects on chlorophyll *a* fluorescence light response curves.

Multiple regression analysis showed a significant effect of the average and variable photon flux densities (PFD_{mean} and PFD_{var}, respectively) on steady state photoprotection (NPQ) and photosystem II (PSII) quantum efficiency (Φ_{PSII}) during a light response curve (Supplemental Fig. 2a-b). As expected, the experimental light intensity (photosynthetic active radiation, PAR) affected NPQ positively and Φ_{PSII} negatively. For NPQ and Φ_{PSII}, a significant interaction between environmental PFD_{mean} and PAR was found, which was negative for NPQ and positive for Φ_{PSII} (statistical analysis in Supplemental Table_SFig2a-b). For Φ_{PSII}, an interaction between environmental PFD_{var} and PAR was found with positive impact. Together, our analyses reveal that the capacity for Φ_{PSII} increases with PFD_{mean} particularly at high PAR, which is accompanied by decreases in NPQ. High PFD_{var} lowers Φ_{PSII} at low to intermediate PAR (Supplemental Table_SFig2a-b). Analysis of covariance including the effects of PFD_{mean} and PFD_{var}, but excluding PAR, separated the different growth environments into groups with DD_F and ND_1 falling together with FD_L, DD_{SF} with FD_M, ND_2 with DD_S and FD_H alone for NPQ light response curves. DD_F organized together with FD_L, ND_1 with DD_{SF}, ND_2 together with FD_M and DD_S, the latter two being in independent groups and FD_H alone for the Φ_{PSII} -light response curves.

Environmental effects on CO_2 assimilation and respiration.

PFD_{mean} was also the main factor explaining differences in whole plant net CO_2 assimilation rates (A_n) between conditions at high and low experimental light intensities, as well as respiration in the dark (R_d; Supplemental Fig. 2c, Supplemental Table_Fig1d_SFig2c). A_n at high irradiance (HI; 900 µmol photons m^{-2} s^{-1}) correlated positively, A_n at low irradiances (LI; 90 µmol photons m^{-2} s^{-1}) negatively and dark respiration again positively with PFD_{mean}, (Supplemental Fig. 2d). PFD_{var} affected HI-A_n positively and R_d negatively. For all three measurements, there was a significant interaction between PFD_{mean} and PFD_{var}. The gross assimilation rate (A_g = HI-A_n+R_d), correlated more strongly with PFD_{mean} than HI-A_n alone (Supplemental Fig. 2e), and showed a near-linear relationship with Φ_{PSII} at maximum PAR, when polytunnel data were excluded (ρ=0.98 and 0.60, respectively). Because day length varied to some extent between ND and phytotron plants, we asked whether correlations of Φ_{PSII} and A_n were stronger for the daily light integral (DLI) or for PFD_{mean}. We found a slightly higher correlation of Φ_{PSII} with DLI (Pearson correlation coefficient ρ=0.835) than with PFD_{mean} (ρ=0.825), while the opposite was observed for A_g, which

correlated more strongly with PFD_{mean} than with DLI (ρ=0.653 and 0.603 respectively). Because differences were minor, all further analyses were conducted with PFD_{mean}.

The Chl *a/b* ratio is positively affected by PFD_{var}.

While protein analyses suggested a negative effect of PFD_{var} on both, the accumulation of the PSI reaction center subunit PsaA and PSII antenna LHCII, the pigment analyses revealed a positive effect of PFD_{var} on the Chl *a*/*b* ratio, which strongly suggests an increase in the reaction center/ antenna ratio as a response to high PFD_{var} (Supplemental Fig. 3-4). One hypothesis that could explain the discrepancy between PFD_{var} effects on protein and pigment results (i.e. no apparent difference in reaction center/ antenna ratio versus an apparent decrease in LHC-bound Chl *b*, respectively), is an increase in Chl *a* binding by antenna proteins as an acclimatory strategy to a fluctuating growth light environment. This hypothesis requires further investigation.

Light intensity and other environmental factors have distinct effects on dynamic NPQ.

To assess the effect of light acclimation on NPQ transients, we determined NPQ during short light fluctuations. NPQ levels increased throughout every HI-phase for all conditions, except for the high-PFD_{mean} conditions FD_H and DD_S. Here, HI-NPQ was lower after 1 min than after 30 s (Supplemental Fig. 5a). Natural environment-grown plants (ND) exhibited the strongest capacity to induce HI-NPQ, followed by DD_F (Supplemental Fig. 5a). We then determined the contribution of fast and slowly relaxing NPQ components (NPQ_f and NPQ_s, respectively; Supplemental Fig. 5b-c) to LI-NPQ at the end of the final fluctuation. NPQ_f largely represents the lumen pH-dependent NPQ component qE and was very similar between all conditions, except for ND_2 with significantly higher values (Supplemental Fig. 5b). When testing for non-linear correlation of NPQ_f with PFD_{var}, we found a significant positive effect (Supplemental Fig. 5f). The NPQ_S amplitude showed a negative dependency on PFD_{mean} and a positive on PFD_{var} (Supplemental Fig. 5f). To quantify the increase of NPQ during the fluctuating light treatment, we performed linear fittings over the last points of each HI- and LI-phase, defining the increase over the respective time periods as ΔNPQ_{LI} and ΔNPQ_{HI} (Supplemental Fig. 5d-e). Differences in ΔNPQ_{LI} and ΔNPQ_{HI} between controlled conditions followed PFD_{mean} similarly to NPQ_s (Supplemental Fig. 5c-e). Correlation analysis revealed a stronger correlation between NPQ_S and ΔNPQ_{LI}, than between NPQ_S and ΔNPQ_{HI}, obtaining Spearman's correlation coefficients of 0.86 and 0.51 (both $p<0.0001$), respectively (Supplemental Fig. 5f-g). Interestingly, plants from both ND trials had high ΔNPQ_{HI} per NPQs, suggesting that their enhanced capacity for fast relaxing HI-NPQ reduces the activation of more slowly relaxing NPQ components (Supplemental Fig. 5h).

Most differences in dynamic NPQ between controlled climate conditions could be related to PFD_{mean}. Acclimation to high PFD_{mean} (i.e. FD_H and DD_S) equipped plants with the capacity to relax photoprotective NPQ during the HI-

phase (Supplemental Fig. 5a) and avoid built up of NPQ_s. Growth at lower PFD_{mean} instead led to a higher accumulation of slowly relaxing NPQ components during the light fluctuations (Supplemental Fig. 5c). An exception was the fast relaxing NPQ component (NPQ_f representing qE) at the end of the final LI phase after 4 fluctuations, which did not correlate with PFD_{mean}, but instead positively with PFD_{var}. Also, more slowly relaxing NPQ components (NPQ_s) increased to some degree with PFD_{var}. Plants from the natural environment had highest capacity for dynamic NPQ (i.e. high HI-NPQ and NPQ_f).